INTRINSIC FEATURE EXTRACTION ON HIPPOCAMPAL SURFACES AND ITS APPLICATIONS

TSZ WAI WONG*, LOK MING LUI†, PAUL M. THOMPSON‡, SHING-TUNG YAU §, AND TONY F. CHAN¶

Abstract. This paper proposes a novel approach to extract two intrinsic feature curves on hippocampal (HC) surfaces. The HC is a key target of study in medical imaging, as it degenerates in conditions such as epilepsy and Alzheimer's disease (AD), but its structure is complex. To facilitate HC morphometry, we generate two intrinsic feature curves that describe their global geometries. For example, the separation of them captures thickness changes in HC surfaces, which can be used to effectively measure HC atrophy found in patients with AD. They also separate HC surfaces into upper and lower surface patches where intrinsic shape analysis using conformal modules can be carried out. Based on these curves, we further propose a parameterization of HC surfaces called the eigen-harmonic parameterization (EHP). EHP maps each HC surface onto a parameter domain and imposes longitudinal and azimuthal coordinates on each surface, which follow the gradient and level-sets of its first non-trivial Laplace-Beltrami eigenfunction respectively. Each tubular domain is constructed according to the geometry of individual HC surface. This gives a parameter domain with much less geometric distortion compared to spherical parameterization. With EHP, all HC surfaces are automatically registered with intrinsic feature curves preserved, and geometric distortions minimized. This allows shape analysis on any number of HC surfaces to be performed consistently. We studied geometric changes over time in 138 HC surfaces of patients with AD and normal subjects scanned at two different times. We successfully located areas with significantly different shape changes over time between the two groups.

Key words. hippocampus, intrinsic feature curve, Laplace-Beltrami eigenfunction, shape analysis

1. Introduction.

The hippocampus (HC) is an important subcortical structure in medical research due to its central role in learning and memory. Its shape and changes over time in diseases such as Alzheimer's disease, epilepsy, and schizophrenia are extensively studied; in addition, the earliest signs of degenerative brain diseases are often first apparent in this area.

Surface-based HC shape analysis is commonly used, where 1-1 registrations between HC surfaces are required. Good registrations are characterized by their smoothness and correspondence of geometric features. Detection and correct localization of shape changes and statistical differences across populations also require accurate mapping of 'landmark lines', which are consistently identifiable anatomical feature curves on biological shapes, such as the sulci and gyri on cortical surfaces. Therefore, many registration algorithms rely on landmark curve correspondences to work properly [21]. However, unless high-field imaging is used, there are no consistently identifiable, well-defined landmarks lines on HC surfaces. This makes accurate surface registration more challenging, when standard brain scanning methods are used (such as T1-weighted MRI at 1.5 or 3 Tesla, which typically uses 1mm cubic voxels). Besides, accurate HC shape morphometry also requires well-defined feature curves that are stable under shape changes, intrinsic to surface geometry and efficient to compute, as a basis for further analysis. However, there is no standard criterion to extract such curves on HC surfaces. In fact, some labor intensive and time consuming approaches have been

*Department of Mathematics, University of California, Los Angeles (alvinwong@math.ucla.edu).
†Department of Mathematics, The Chinese University of Hong Kong (lmlui@math.cuhk.edu.hk).
‡Laboratory of Neuro Imaging, UCLA School of Medicine (thompson@loni.ucla.edu).
§Department of Mathematics, Harvard University (yau@math.harvard.edu).
¶Hong Kong University of Science and Technology (tonyfchan@ust.hk).

proposed, that attempt to manually landmark curves on unfolded HC surfaces [32] [2].

Although these have advanced brain research [33], the need for expert intervention makes them impractical to use in samples of more than a few brain scans. Instead, most high-throughput HC morphometry approaches in large samples of subjects have used simple parameterizations that ignore intrinsic surface landmarks [17] [18] [20]. To tackle this problem, in this paper we make contributions in three key areas. First, we propose an algorithm that automatically extracts two precisely defined intrinsic feature curves on each HC surface based on intrinsic surface geometry. Second, we further propose a complete parameterization of the whole HC surface based on these curves. This automatically gives a smooth, one-to-one, point-to-point correspondence on all HC surfaces for shape analysis. Finally, to make our parameterizations smoother and reduce distortion, we define a parameter domain according to the shape of each HC surface, so that our parameterization onto the domain can be smoothed and optimized to geometry.

With the resolution and image contrast typically obtained with standard T1-weighted brain MRI at 1.5 or 3 Tesla, the HC surface as a whole takes the shape of a flattened and curved tube. We identify two ridge feature curves of this shape, one lying on the inner curved region and the other lying on the outer curved region (see Figure 4.2). Both of them proceed in the longitudinal direction. To extract these two features, one needs a function that 'understands' the geometry of HC surfaces – the first non-trivial eigenfunction of the Laplace-Beltrami (LB) operator on the surface.

The LB operator is an intrinsic operator defined on Riemannian manifolds, invariant to the embedding of these surfaces in Euclidean space. Reuter et al. [23] [22] proposed to use its eigenfunctions for shape analysis. In particular, its first non-trivial eigenfunction has the property of monotonically increasing its value from one end to the other end of elongated shapes like HC surfaces. With this property, and noting that the two feature curves proceed in the longitudinal direction, they must intersect each eigen-loop at exactly two points. This enables us to propose a variational approach to construct these curves by extracting a pair of points on each eigen-loop and joining the points on the same side.

Using the two feature curves, we construct a shape indicator by computing the separation between them at different locations of HC surfaces. This gives a robust measure of the 'thickness' of HC surfaces in different areas. We demonstrate that the shape indicator can effectively detect atrophy in HC surfaces by comparing normal subjects with AD patients. Furthermore, the landmarks divide HC surfaces into upper and lower patches. By mapping these patches conformally onto rectangles, we compute the conformal modules of these patches, which are important indicators for shape analysis.

Finally, we apply the extracted feature curves on HC surface registration. Using the feature curves and eigen-loops, we construct a parameter domain according to the geometry of each HC surface, which is parameterized by longitudinal (α) and azimuthal (θ) coordinates. We map each HC surface onto its domain using a normalized LB eigenfunction as the longitudinal coordinate, and map the intrinsic feature curves onto $\theta = 0$ and $\theta = \pi$. To further optimize the parameterization, we minimize the harmonic energy of map from the HC surface onto its parameter domain. Our results show that this parameterization, also called the eigen-harmonic parameterization (EHP), is smooth, and gives much less geometric distortions compared to the widely used method of mapping HC surfaces onto spheres. Using EHP, all HC sur-

faces are automatically registered under a consistent parameterization optimized for geometry. This allows us to perform shape analysis on any number of HC surfaces. In our experiment, we compute the EHP of 478 HC surfaces acquired from 93 patients with Alzheimer's disease and 146 normal subjects at two different times. By analyzing the temporal geometric changes of 138 random HC surfaces in these subjects, we successfully locate areas with statistically significant shape changes between two groups.

2. Previous Work. Hippocampus has been widely studied in medical research for shape analysis in normal subjects, people with disabilities such as blindness [10], and in diseases such as Alzheimer's [27] and epilepsy [11]. As in the study of cortical surfaces, accurate registration is vital in improving the power to detect differences between groups and for creating classifiers that attempt to automatically assign individuals to diagnostic groups based on their imaging measures. Many different methods of surface-based registration exist in the current literature. Thompson et al. proposed to parameterize cortical surfaces onto spheres [26]. They further proposed using the spherical parameterization to create brain atlases that describe variations of a group of cortical surfaces over time [28]. Gu et al. [6][30] proposed to register cortical surfaces conformally onto a sphere or a disk for further analysis. Lord et al. [12] proposed to register surfaces by minimizing an energy functional describing local metric changes. Other methods have also been used, such as driving surface registrations using mutual information on surfaces [29], and finding landmark-matching diffeomorphic deformations by modeling sulcal lines as 'currents' [4].

While surfaces from medical imaging can be registered based only on geometric features extracted from surface (e.g., the local surface curvature or metric), the results may not agree well with the anatomical landmarks that would be recognized and labeled by an anatomist or radiologist. Therefore, landmark lines labeled by researchers expert in anatomy are important to guide the registration process. For instance, Lui et al. [15] used a variational approach to compute an optimized conformal registration that aligns landmarks as well as possible. However, landmarks are not matched exactly and diffeomorphisms cannot be guaranteed when there is a large number of landmarks. In [13], they further computed shape-based landmark matching registrations between brain surfaces using a method called the integral flow method. The one-parameter subgroup within the set of all diffeomorphisms was considered, and the one parameter subgroup was represented by smooth vector fields. Landmarks can be perfectly matched and the correspondence between landmark curves is based on the shape information. Joshi et al. [8] proposed to register cortical surfaces by minimizing a harmonic energy function in the p-th norm. A related method was applied by Shi et al. [25] to match implicitly-defined surfaces by solving PDEs on them using level set methods. Leow et al. [9] proposed a feature-based brain image warping approach by a hybrid implicit/explicit framework and applied it on corpus callosums and cortical surfaces. In general, landmark-based methods are more accurate as they make use of the information from anatomically trained researchers, but the manual labeling of surfaces is time-consuming and prohibitive in larger projects.

When there are no well-defined landmark lines from trained anatomists, as is usually the case for HC surfaces, one has to look for more information in the geometry of the shapes. Lui et al. [16] proposed to look for an optimized geometric matching registration between HC surfaces by minimizing a complete shape energy, which is defined by the Beltrami coefficient and curvatures. Reuter et al. [23] proposed shape analysis using LB spectra of shapes, as they are almost unique to each shape except

in rare exceptional cases constructed artificially. Shi et al. [24] further proposed using LB eigenfunctions to find landmark lines on HC surfaces and map them onto a sphere for HC registration. The end points of the landmark curves are based on geodesic transforms, which can be sensitive to local geometric changes. Hence, the extracted landmarks are sensitive to noise. Also, a sphere has a different geometry from HC surfaces and is not elongated like HC surfaces. This results in large distortions for some cell sizes in the imposed parametric grid, especially near the poles of the sphere. Landmark detection based on more direct geometric quantities such as curvature has also been proposed by Yoshizawa et al. [31]. Later, Lui et al. [14] also proposed to trace sulci landmarks on brain cortical surfaces based on the mean curvature and principal curvatures. In general, methods based on curvature can be sensitive to subtle surface changes such as bumps, and may wrongly detect them as feature curves on HC surfaces. Some regularization is necessary.

3. Theoretical Background and Terminology. In this section, we present the theory of LB eigenfuctions, which enables us to extract intrinsic feature curves on HC surfaces.

3.1. The Laplace-Beltrami Operator and its Eigenfunctions. In differential geometry, the Laplace-Beltrami operator is well-studied [1][3]. Given a function $f\colon M \to \mathbb{R}$ on a Riemannian manifold M, the operator is defined as the divergence of the gradient: $\Delta f = \operatorname{div} \operatorname{grad} f$. On compact manifolds, the operator has a discrete spectrum $0 \leq \lambda_1 \leq \lambda_2 \leq \cdots \uparrow \infty$. We are interested in its first non-trivial eigenfunction $f\colon M \to \mathbb{R}$, satisfying $-\Delta f = \lambda f$ and $\lambda > 0$. The function is smooth and minimizes the harmonic energy functional: $f = \arg\min_{\|f\|=1} \int_M \|\nabla_M f\|^2$. In some sense, it is the 'least expanding' map in orthogonal directions.

On a Riemann surface, its first non-trivial LB eigenfunction carries much geometric and topological information, such as the branching and genus of the surface. For example, if $f\colon M \to \mathbb{R}$ is such an eigenfunction on Riemann surface M of genus g, then f has at least $2g+2$ critical points. The number of critical points is stable under small changes in the surface metric. Therefore, the eigenfunctions on similar surfaces have the same number of critical points. On a simply-connected closed surface such as the HC surface, their first non-trivial LB eigenfunctions always increase from one tip to the other. There are always two critical points located at the two tips of the HC surface. This gives us a longitudinal coordinate on the HC surface, and enables us to map each HC surface onto a tube-like domain, given by the following theorem:

THEOREM 3.1. *Let M be a smooth manifold and $f\colon M \to \mathbb{R}$ be a smooth function. Assume f has exactly two critical points $p_1, p_2 \in M$ with $f(p_1) < f(p_2)$. Pick some $\varepsilon < (f(p_2) - f(p_1))/2$. Then $f^{-1}([f(p_1) + \varepsilon, f(p_2) - \varepsilon])$ is diffeomorphic to $I \times S^1$, where $I = [f(p_1) + \varepsilon, f(p_2) - \varepsilon]$ and S^1 is a circle.*

By the theorem, there exists a smooth mapping from $I \times S^1$ to $f^{-1}(I)$, where $I = [a, b]$ is an interval inside the range of the eigenfunction f excluding the two critical points, i.e. $I \subseteq f(M \backslash \{p_1, p_2\})$. This allows us to parametrize HC surfaces into longitudinal and azimuthal coordinates.

4. Our Proposed Framework and Algorithms. In this section, we explain in detailed how the two intrinsic feature curves can be computed on each HC surface. This leads to a full parameterization defined at every point on the surface. To give readers some idea about this process, we first give an overview of our proposed framework in Subsection 4.1. After that, we describe every step and our algorithms in detail.

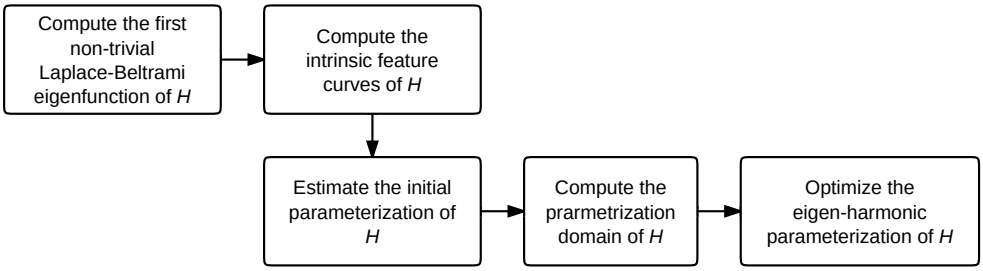

FIG. 4.1. *Our proposed procedures for parameterizing a HP surface H.*

4.1. An Overview of Our Proposed Framework. In order to compute two intrinsic feature curves on a HC surface, we need a robust method to obtain the correct orientation of the HC surface, such as distinguishing the head and tail tips of the HC surface. As discussed in Section 1, the first nontrivial LB eigenfunction 'understands' the geometry of the HC surface and is suitable for this purpose. It will also be used to construct the longitudinal parameterization of the whole HC surface. Due to the shape of the HC surface, every eigen-loop of the function is simply connected and intersects with the two intrinsic feature curves at exactly two points. In Subsection 4.2, we precisely define these curves and discuss an algorithm for extracting them.

Once the two intrinsic feature curves are computed, we begin to compute a global parameterization for the HC surface. After a normalization process, the LB eigenfunction is used as the longitudinal coordinate α, which maps the HC surface onto $[0, 1]$. At the same time, we also give every point on the HC surface an azimuthal coordinate θ according to its location with respect to the feature curves, which lies in $[0, 2\pi)$. This is a preliminary parameterization of the HC surface onto $[0, 1] \times [0, 2\pi)$ and will be discussed in Subsection 4.3.

After a preliminary parameterization is computed, it is time to optimize the parameterization so that the same coordinate on all HC surfaces corresponds well. We aim to minimize the unevenness that may have occurred in the preliminary parameterization process, and at the same time preserve geometric information well. To meet these goals, we construct a parameter domain based on the geometry of the HC surface, but with a well-defined parameterization on $[0, 1] \times [0, 2\pi)$. The parameterization of the HC surface induces a diffeomorphic map onto the parameter domain. The map can be optimized to improve the parameterization of the HC surface. Details of the construction of the domain are given in Subsection 4.4.

Finally, in Subsection 4.5, we discuss how the parameterization can be optimized by minimizing the harmonic energy of the map from the HC surface onto its parameter domain. This completes the whole process of extracting two intrinsic feature curves and computing a consistent global parameterization on all HC surfaces. Since the HC surface is not very convoluted, exponential maps may be used to give good parameterizations locally. However, since we aim at obtaining a consistent global parameterization across all subjects, harmonic maps are more appropriatefor this goal. A flowchart summarizing our procedures is presented in Figure 4.1.

4.2. Intrinsic Feature Extraction from LB Eigenfunctions. Given a HC surface H. Let $f : H \to \mathbb{R}$ be its first non-trivial LB eigenfuction. f satisfies $-\Delta f = \lambda f$, where λ is the first non-zero eigenvalue of the LB operator. We propose to extract two intrinsic feature curves from H using the eigenfunction f. Since the HC surface

H takes the shape of an elongated tube, f is a smooth function on H with exactly two critical points at its tips. We aim to locate two intrinsic feature curves that lie on the opposite sides of the most curved regions of H and go along the longitudinal direction. Therefore, they must intersect with each eigen-loop at exactly two points. Motivated by this observation, we define the intrinsic feature curves as follows:

DEFINITION 4.1. *Let H be a HC surface in $\mathbb{R}^3$ and $f\colon H \to \mathbb{R}$ be its first non-trivial LB eigenfunction, with $f(H) = [a, b]$. Then we define the intrinsic feature curves on H to be the curves $\gamma_1, \gamma_2\colon [a, b] \to H$ such that*

$$\{\gamma_1, \gamma_2\} = \operatorname{argmax} \frac{1}{b-a} \int_a^b |\gamma_1(t) - \gamma_2(t)|\, dt - c_1 \int_a^b |\dot{\gamma_1}(t)|\, dt - c_2 \int_a^b |\dot{\gamma_2}(t)|\, dt, \quad (4.1)$$

where $c_1, c_2 \geq 0$ are user parameters.

The motivation of this definition is that the feature curves should be separated as much as possible since the two ridges along the sides of the HC surfaces are opposite to each other. Therefore the first term representing their average separation should be minimized. The second and third terms represent the lengths of the feature curves and are added to regulate their smoothness. In our experiments, we set c_1 and c_2 to 0.5 to put more emphasis on the average separation of the curves.

We discretize the two feature curves by $V = \{v_0, \ldots, v_n\}$ and $W = \{w_0, \ldots, w_n\}$ on H, where $f(v_0) = f(w_0) = a$, $f(v_n) = f(w_n) = b$, and $f(v_i) - (v_{i-1}) = f(w_i) - (w_{i-1}) = (b-a)/n$ for all i. This implies $f(v_i) = f(w_i) = a + i(b-a)/n$ for $i = 0, 1, \ldots, n$. Initially, we take v_i, w_i to be the furthest pair of points on their corresponding eigen-loop $f^{-1}(a+i(b-a)/n)$. The discrete version of the minimization problem becomes:

$$\{V, W\} = \operatorname{argmax} \frac{1}{n+1} \sum_{i=0}^{n} |v_i - w_i| - c_1 \sum_{i=0}^{n-1} |v_{i+1} - v_i| - c_2 \sum_{i=0}^{n-1} |w_{i+1} - w_i|. \quad (4.2)$$

Let $E(V, W)$ be the energy functional in (4.2). To optimize this energy functional, we look for directions $\{\alpha_0 d_0, \ldots, \alpha_n d_n\}$ and $\{\beta_0 e_0, \ldots, \beta_n d_n\}$ such that $V_{tmp} = \{v_0 + t\alpha_0 d_0, \ldots, v_n + t\alpha_n d_n\}$ and $W_{tmp} = \{w_0 + t\beta_0 e_0, \ldots, w_n + t\beta_n e_n\}$ give the steepest descent to (4.2) for small $t > 0$, where d_i's and e_i's are unit tangential vectors along the eigen-loops containing v_i's and w_i's respectively, α_i's and β_i's are the amounts of descent for v_i's and w_i's respectively, which will be computed in the appendix. The algorithm is summarized in Algorithm 1.

We illustrate the first non-trivial LB eigenfunction of a HC surface, its eigen-loops and two initial intrinsic feature curves in Figure 4.2. The final curves will be illustrated in Section 5.

4.3. Estimating the Initial Parameterization. In this subsection, we give an initial global parameterization for a HC surface H. As its first non-trivial LB eigenfunction f increases its value from one tip to another tip, we can normalize f and use it as the longitudinal coordinate function of H. Let $f(H) = [a, b]$. We change the sign of f if necessary such that f takes smaller values near the slimmer tip and bigger values near the fatter tip (as in Figure 4.2). Then we define the longitudinal coordinate function $\alpha\colon H \to [0, 1]$ by

$$\alpha(v) = \frac{f(v) - a}{b - a}. \quad (4.3)$$

Algorithm 1 Compute two intrinsic feature curves from a HC surface H

Require: A HC surface H and its first non-trivial LB eigenfunction f, $f(H) = [a, b]$
  Set $n = 100$;
  for all $i = 0, 1, \ldots, n$ **do**
    Compute the pair of furthest points v_i and w_i on eigen-loop $f^{-1}(a + i(b-a)/n)$;
  end for
  Set $V = \{v_0, \ldots, v_n\}$, $W = \{w_0, \ldots, w_n\}$;
  Set step size $t = 0.01$;
  repeat
    Compute the tangential directions d_i's and e_i's for all v_i's and w_i's respectively;
    Set $V_{tmp} = \{v_0 + t\alpha_0 d_0, \ldots, v_n + t\alpha_n d_n\}$, $W_{tmp} = \{w_0 + t\beta_0 e_0, \ldots, w_n + t\beta_n d_n\}$;
    Compute α_i's and β_i's that give the steepest descent to $E(V_{tmp}, W_{tmp})$;
    Update V and W using V_{tmp} and W_{tmp} with α_i, β_i and step size t;
  until improvement in the energy functional over the last 50 iterations < 0.001 (mm).

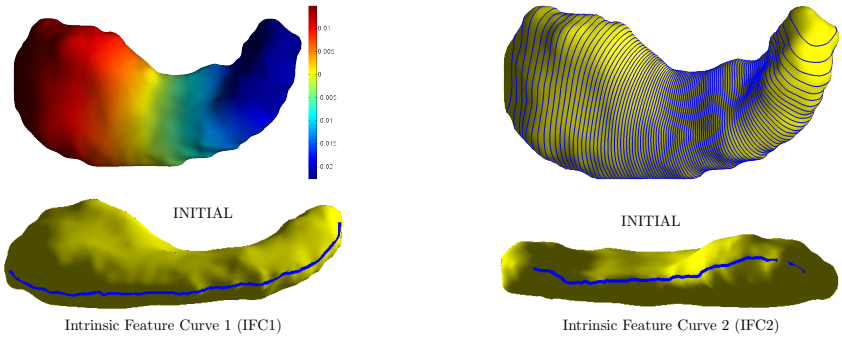

FIG. 4.2. *The color-map of the first non-trivial LB eigenfunction of a HC surface, its level-sets and the initial intrinsic feature curves.*

α is a normalization of f that parameterizes H longitudinally onto $[0, 1]$. It has the same level-sets as f, which are also closed curves called eigen-loops. To obtain a global parameterization of H, we further define an azimuthal coordinate function $\theta \colon H \to [0, 2\pi)$ for every point on H according to its position on its eigen-loop.

To begin with, we label the two intrinsic feature curves we computed on H. The longer curve lies on the outer side of human brain and is labeled as IFC1, while the shorter curve lies on the inner side of human brain and is labeled as IFC2. We aim to parameterize H such that $\theta = 0$ on IFC1 and $\theta = \pi$ on IFC2. Points on every eigen-loop are parameterized from 0 to 2π according to the right-hand rule, with the thumb pointing to the direction u of increasing α. Our labelings of the two intrinsic feature curves are shown in Figure 4.2 and the direction of increasing θ is shown in Figure 4.3.

Given a point v on H, let Γ be the eigen-loop v lies on, i.e., $\Gamma = \alpha^{-1}(\alpha(v))$. We locate points p_1, p_2 on Γ where it intersects with IFC1 and IFC2 respectively. Let m be the mid-point of p_1 and p_2. We compute the angle σ segment $\{v, m\}$ makes with $\{p_1, m\}$. If $\{p_1 - m, v - m, u\}$ is positively oriented, we set $\theta(v) = \sigma$. Otherwise, we set $\theta(v) = 2\pi - \sigma$. The algorithm is summarized in Algorithm 2. For better illustration, in Figure 4.3, we label the variables used by the algorithm to compute $\theta(v)$ for a

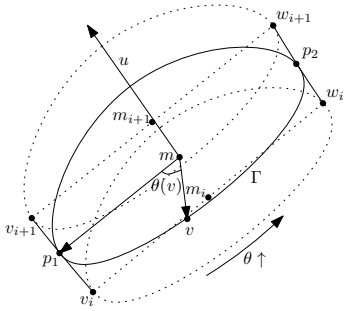

FIG. 4.3. *The variables used in Algorithm 2 to compute $\theta(v)$ for every vertex v on a HC surface and the direction of increasing θ.*

vertex v.

Algorithm 2 Compute an initial azimuthal parameterization θ on a HC surface H

Require: A HC surface H represented by a triangular mesh $(\mathcal{V}, \mathcal{E}, \mathcal{F})$, its two intrinsic feature curves IFC1 and IFC2 represented by $V = \{v_0, \ldots, v_n\}$ and $W = \{w_0, \ldots, w_n\}$ respectively, its longitudinal parameterization $\alpha \colon H \to [0, 1]$

for all $v \in \mathcal{V}$ **do**

$i = \lfloor n\alpha(v) \rfloor$;

$m_i = (v_i + w_i)/2$;

$m_{i+1} = (w_{i+1} + w_{i+1})/2$;

$u = (m_{i+1} - m_i)/\left\|m_{i+1} - m_i\right\|$;

$\Gamma = \alpha^{-1}(\alpha(v))$;

$\sigma = \text{acos}[(v - m) \cdot (p_1 - m)/\left\|v - m\right\| \left\|p_1 - m\right\|]$;

Compute the intersections p_1 and p_2 of Γ with V and W respectively;

if $\det[p1 - m, v - m, u] > 0$ **then**

Set $\theta(v) = \sigma$;

else

Set $\theta(v) = 2\pi - \sigma$;

end if

end for

The initial parameterization of H using α and θ is global and carries a geometric interpretation. However, to justify that it is robust, we need a standard measure and compare it with other methods. In the next subsection, we construct a parameter domain according to the geometry of H and define what this measure is. After that, we can measure how good our parameterization is and optimize it accordingly.

4.4. A Parameter Domain for HC Surfaces. In this subsection, we construct a parameter domain for a HC surface H. In this way, our parameterization in Subsection 4.3 is realized as a mapping from H onto it. This gives our parameterization a well-defined geometric meaning and allows us to measure its robustness. Further optimization can then be applied.

To construct a parameter domain for H, we look for a surface that has a similar geometry to H and can be easily parameterized. Since every eigen-loop of H is a closed curve resembling an ellipse, we construct a tube-like domain where every cross section is an ellipse. We aim to map H onto this domain so that every eigen-loop is mapped

onto an elliptic cross section. The eccentricity of every such cross section is determined by the corresponding eigen-loop. The height h of the parameter domain is given by the length of a medial axis of H, which is computed from the mid-points of the corresponding points in IFC1 and IFC2. Using the parameterization constructed in Subsection 4.3, a point v in H is mapped to the point $(a(v)\cos(\phi(v)), b(v)\sin(\phi(v)), h\alpha(v))$ on the parameter domain, where $a(v)$ and $b(v)$ depend on the shape of the ellipse, and $\phi(v)$ is computed such that $(b(v)\tan(\phi(v))/a(v) = \tan(\theta(v))$, and $\cos(\phi(v))$ and $\cos(\theta(v))$ take the same sign. We construct the parameter domain K and map H onto it using Algorithm 3.

Algorithm 3 Construct and map a HC surface H onto its parameter domain K by defining $\Phi\colon H \to K$

Require: A HC surface H represented by a triangular mesh $(\mathcal{V}, \mathcal{E}, \mathcal{F})$, its two intrinsic feature curves IFC1 and IFC2 represented by $V = \{v_0, \ldots, v_n\}$ and $W = \{w_0, \ldots, w_n\}$ respectively, its initial parameterization by $\alpha\colon H \to [0,1]$ and $\theta\colon H \to [0, 2\pi)$

for all $i = 0, 1, \ldots, n$ **do**
  $m_i = (v_i + w_i)/2$;
end for
h =length of $\{m_0, m_1, \ldots, m_n\}$;
for all $v \in \mathcal{V}$ **do**
  $\Gamma = \alpha^{-1}(\alpha(v))$;
  Compute the intersections p_1 and p_2 of Γ with V and W respectively;
  $a(v) = \|p_1 - p_2\|/2$;
  Compute $b(v)$ such that the ellipse $\{(x/a(v))^2 + (y/b(v))^2 = 1\}$ has the same perimeter as Γ;
  $\phi(v) = \arctan(a(v)\tan(\theta(v))/(b(v))$;
  Add π or 2π to $\phi(v)$ such that $\phi(v) \geq 0$ and $\cos(\phi(v))$ and $\cos(\theta(v))$ take the same sign;
  $\Phi(v) = (a(v)\cos(\phi(v)), b(v)\sin(\phi(v)), h\alpha(v))$;
end for
K is given by the triangular mesh $(\Phi(\mathcal{V}), \mathcal{E}, \mathcal{F})$.

Formally, K is a closed surface in $\mathbb{R}^3$ with height h. The intersection of K with $z = c$ is $\{(x/a)^2 + (y/b)^2 = 1, z = c\}$, where the values of a and b are taken respectively as $a(v)$ and $b(v)$ computed in the loop of the algorithm by setting $\Gamma = \alpha^{-1}(c/h)$. Also note that we may equivalently parameterize K by α and θ instead of α and ϕ. Since the angle θ can be intuitively given in Figure 4.3, we will use θ for our registration, but will use ϕ for the optimization of our parameterization for easy computation. The algorithm allows us to consider the initial parameterization in Subsection 4.3 as a mapping from H onto K. This enables us to define the smoothness of our parameterization and further optimize it. In the next subsection, we discuss how our parameterization can be further optimized to give the final parameterization of H.

4.5. The Eigen-Harmonic Parameterization of HC Surfaces. At this point, we have computed an initial global parameterization of a HC surface H onto $\{(\alpha, \theta) \in [0,1] \times [0, 2\pi)\}$, which is also a mapping from H onto a parameter domain K. In this section, we further optimize our parameterization to give a final parameterization of H.

To further improve the mapping from H onto K, we define a good mapping to be

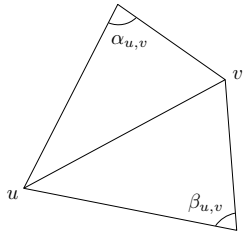

FIG. 4.4. *Angles defined in the cotangent-weight Laplacian operator.*

one that induces the least amount of distortion in the mapping. A widely accepted measure is the harmonic energy of the mapping. Since H and K are both simply-connected closed surfaces, the mapping with the least harmonic energy is a conformal mapping preserving angles. Therefore, if we optimize its harmonic energy by changing both α and θ, the mapping becomes conformal and the motivation to parameterize H using its first non-trivial LB eigenfunction is lost. To avoid this problem, we optimize the harmonic energy by adjusting θ. We also require that IFC1 and IFC2 to be mapped onto $\{\theta = 0\}$ and $\{\theta = \pi\}$ on K. The final parameterization is defined as follows:

DEFINITION 4.2. *Let H be a HC surface, Γ_1 and Γ_2 be its IFC1 and IFC2 respectively, and K be its parameter domain, which is equivalent to $\{(\alpha, \theta) \in [0, 1] \times [0, 2\pi)\}$. We define the final parameterization of H as the mapping $\Phi \colon H \to K$ such that*

$$\Phi = \operatorname{argmin}_{\Phi(\Gamma_1)=\{\theta=0\},\Phi(\Gamma_2)=\{\theta=\pi\}} \int_H \|\nabla \Phi\|^2 . \tag{4.4}$$

Φ is called the eigen-harmonic parameterization (EHP) of H.

Using EHP, a consistent coordinate system (α, θ) can be given on every HC surface H. To compute the final Φ in a discrete setting, we start from the initial parameterization Φ given in Algorithm 3 for a HC surface represented by a triangular mesh $(\mathcal{V}, \mathcal{E}, \mathcal{F})$. We define the cotangent-weight Laplacian operator:

$$L_{u,v} = \begin{cases} \frac{1}{2}(\cot(\alpha_{u,v}) + \cot(\beta_{u,v})) & \text{if } u \neq v \text{ and } u \in \mathrm{Nbr}(v), \\ -\sum_{w \in \mathrm{Nbr}(v)} L_{u,w} & \text{if } u = v, \\ 0 & \text{otherwise,} \end{cases} \tag{4.5}$$

where $\alpha_{u,v}$ and $\beta_{u,v}$ are defined for an edge $(u, v) \in \mathcal{E}$ as in Figure 4.4. This formula can be derived from finite element analysis [7].

Let $\Phi = (\Phi_1, \Phi_2, \Phi_3)$. The discretization of the energy in (4.4) is given by

$$E(\Phi) = \sum_{i=1}^{3} E_{\mathrm{harmonic}}(\Phi_i), \tag{4.6}$$

where E_{harmonic} is defined as

$$E_{\mathrm{harmonic}}(f) = \frac{1}{2} \sum_{u,v \in V} L_{u,v} \cdot (f(u) - f(v))^2 \tag{4.7}$$

for a function $f \colon V \to \mathcal{R}$. This energy is a standard discretization of the harmonic energy and can be easily minimized using gradient descent.

We minimize E by optimizing the function ϕ in the (α, ϕ) parameterization of H in Algorithm 3. Since we are keeping α fixed, we may write E as $E(\phi) = E(\phi_1, \phi_2, \ldots, \phi_m)$, where m is the number of vertices in $\mathcal{V} = \{v_1, v_2, \ldots, v_m\}$ and $\phi_i = \phi(v_i)$ for $i = 1, 2, \ldots, m$. To optimize E, we look for adjustments δ_i's such that $(\phi_1 + t\delta_1, \ldots, \phi_m + t\delta_m)$ give the steepest descent to E for small $t > 0$. The descent direction will be given in the appendix. To map IFC1 and IFC2 onto $\{\theta = 0\}$ and $\{\theta = \pi\}$ respectively, we simply fix every $\phi(v_i)$ with v_i on IFC1 or IFC2. The algorithm is summarized in Algorithm 4.

Algorithm 4 Compute the eigen-harmonic parameterization of a HC surface H

Require: A HC surface H represented by a triangular mesh $(\mathcal{V}, \mathcal{E}, \mathcal{F})$, its two intrinsic feature curves IFC1 and IFC2, its initial parameterization by $\alpha\colon H \to [0, 1]$ and $\theta\colon H \to [0, 2\pi)$
Compute $\phi\colon H \to [0, 2\pi)$ from θ;
repeat
Compute δ_i's that give the steepest descent to $E(\phi_1 + t\delta_1, \ldots, \phi_m + t\delta_m)$;
Update every $\phi(v_i)$ such that v_i is not on IFC1 or IFC2 using $\phi_i + t\delta_i$ with step size t;
until improvement in the energy functional over the last 50 iterations $< 0.01\%$;
Update θ using ϕ.

Using this algorithm, we obtain the EHP for every HC surface H, which is the least distorted mapping from H onto its parameter domain K. This gives H a global parameterization onto $\{(\alpha, \theta) \in [0, 1] \times [0, 2\pi)\}$. EHP carries intrinsic geometric meaning and automatically registers every pair of HC surfaces H_1 and H_2. This allows us to compute shape changes from H_1 to H_2 precisely by comparing the corresponding changes in geometric quantities from H_1 to H_2, such as the mean curvature and Gaussian curvature. In the next section, we present our experimental results and show how this method can be used for HC morphometry.

5. Experimental Results. In this section, we present our results on the extraction of intrinsic feature curves, global parametrization of HC surfaces and its optimization to give eigen-harmonic parameterizations. We demonstrate the convergence of our algorithms and their use for HC morphometry. Experiments were carried out on 478 HC surfaces automatically extracted from 3D brain MRI scans of 239 patients at two different times (the baseline time-point and 12 months after). Scans were acquired from 146 normal and 93 diseased (AD) elderly subjects on an 1.5T GE Signa scanner, and the HC was automatically segmented from each brain scan using a machine learning approach based on adaptive boosting [19] [17]. All computations were programmed in MATLAB with MEX functions for labor-intensive tasks and performed on a laptop with a 1.86GHz Intel Core 2 Duo processor and 2GB of RAM.

5.1. Intrinsic Feature Curves as Shape Indices. Before we use Algorithm 1 to extract two intrinsic feature curves on a HC surface H represented by a triangular mesh $(\mathcal{V}, \mathcal{E}, \mathcal{F})$, we need to compute its first non-trivial LB eigenvalue. We discretize the LB operator on H using the widely used cotangent formula derived from finite element analysis [7], which is symmetric positive semidefinite in matrix form. We compute its first non-trivial eigenfunction using an efficient algorithm by Golub et al. [5] for symmetric matrices, which normally takes less than 5 seconds. After that, we compute two intrinsic feature curves from H.

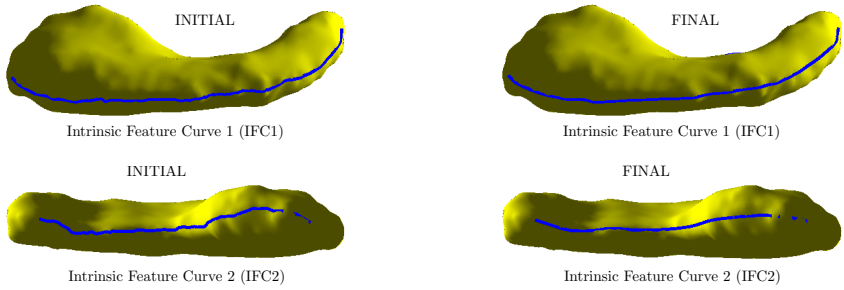

FIG. 5.1. *A comparison of the initial intrinsic feature curves (left) and the final intrinsic feature curves (right) extracted from a HC surface.*

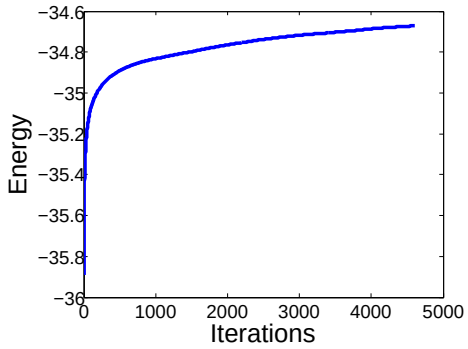

FIG. 5.2. *A plot of the energy functional against the number of iterations in computing the intrinsic feature curves in Figure 5.1.*

The result of our algorithm is shown in Figure 5.1. Initially the intrinsic feature curves extracted were not smooth and showed occasional jumps on H. After optimizing the energy functional in Equation (4.2), the resulting curves lie on the most curved regions of the HC surface with greatly improved smoothness. A plot of the energy functional against the number of iterations is shown in Figure 5.2. In this example, our algorithm converges successfully on H. On all other HC surfaces we tested, similar results were observed.

The intrinsic feature curves may be used to extract geometric information from HC surfaces. In this test, we cut the regions of HC surfaces with α in $[0.01, 0.99]$ into two patches using the curves, namely the front and back patches. Then each patch is mapped conformally onto a rectangle, with the height to width ratio invariant up to conformal deformations. This is an intrinsic surface property of the patch called conformal module [34], which tells us about the thickness to length ratios of HC surfaces. In Figure 5.3, the top and bottom patches of two groups of HC surfaces (AD and normal) are mapped conformally onto rectangles, with the conformal modules computed. The conformal modules of the AD subjects are smaller than that of the normal subjects at different degrees, suggesting a smaller thickness to length ratios for the HC surfaces in the AD subjects. This can be used by neuroscientists to determine the location of atrophy in HC surface deformations.

To demonstrate the robustness of the extraction of the intrinsic feature curves, we illustrate the results of our algorithm for two HC surfaces in Figure 5.4. One HC surface was picked from the AD group and the other from the normal group. For

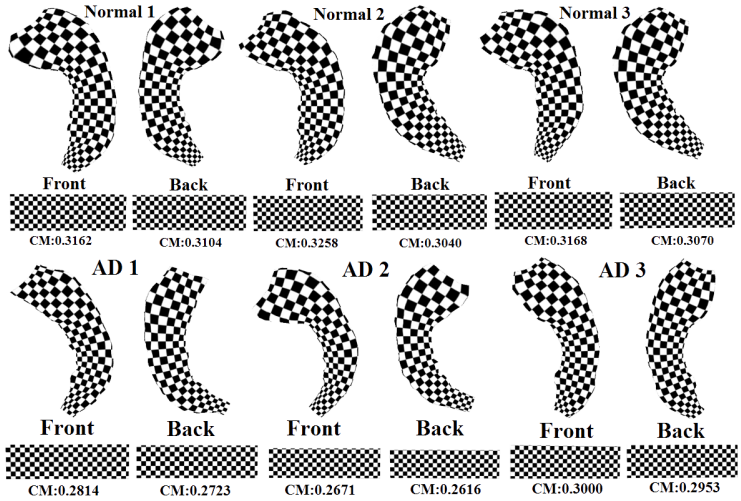

FIG. 5.3. *The conformal modules of the upper and lower patches in HC surfaces of normal and AD subjects.*

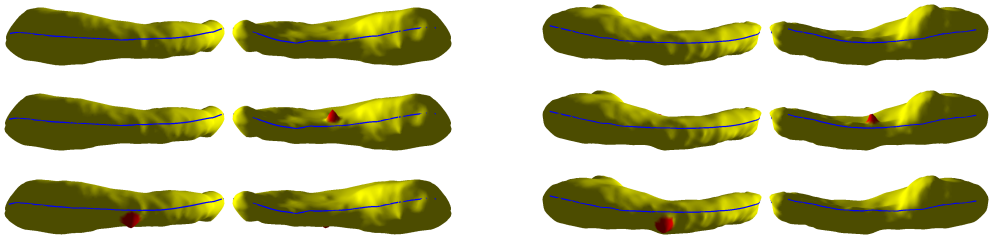

FIG. 5.4. *The results of the extraction of intrinsic feature curves on two HC surfaces. On the left, the front and back of an HC surface from the AD group and two deformations by adding a bump near each intrinsic feature curve are plotted with the extracted intrinsic feature curves marked in blue and the bump in red. The figures on the right show the corresponding results for an HC surface from the normal group. The intrinsic feature curves are stable and not seriously affected by the bumps.*

each HC surface, we test our algorithm on the original surface, and two deformed HC surfaces by adding a bump very near one intrinsic feature curve. As shown in Figure 5.4, only mild changes to the intrinsic feature curves was observed. The results on other HC surfaces also show only mild changes to these curves on the deformed surfaces. This demonstrates the robustness of our algorithm under bumps in the data.

Similarly, we test for the robustness of the intrinsic feature curves under noise. In this test, we add evenly distributed noises in normal direction to the surface data, making the surface uneven and jaggy. An example of this is shown in Figure 5.5. We compare the extracted intrinsic feature curves on the original HC surface and those from the noisy HC surface. It is found that even with noises added to all surface data, the extracted intrinsic feature curves still look very close to those in the original surface. Similar results are found on other HC surfaces. This shows that our algorithm is also robust to noises in the surface data.

5.2. Initial Global Parameterization and its Optimization. In Subsection 4.3, we proposed an initial global parameterization of a HC surface. We constructed

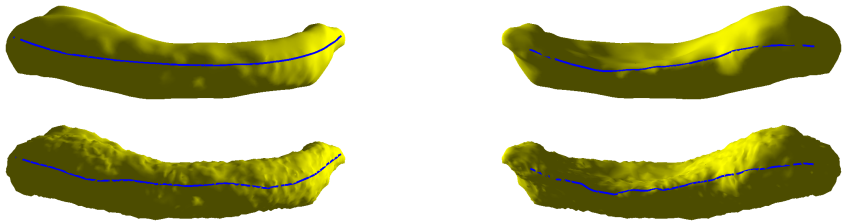

FIG. 5.5. *The results of the extraction of intrinsic feature curves on a HC surface and the same surface with noise. In the upper figures, the front and back of the original HC surface are plotted with the extracted intrinsic feature curves marked in blue. In the lower figures, the front and back of the HC surface with noise in normal direction are plotted with the extracted intrinsic feature curves marked in blue. Only mild changes are observed in the extracted intrinsic feature curves.*

(a) (b) (c)

FIG. 5.6. *The initial estimation of θ and its optimization. (a) shows a HC surface textured with the final parameterization. (b) shows its parameter domain and one of its tip under the mapping of the HC surface using the initial estimation of θ. (c) shows the parameter domain and its tip under the final mapping using the optimized θ.*

a parameter domain to realize it as a mapping in Subsection 4.4 and optimized this parameterization in Subsection 4.5. In this subsection, we discuss the results of these procedures.

For consistency, we continue to use the HC surface H in Subsection 5.1 for illustration. In Figure 5.6(a), we plot H and texture it with a checkerboard pattern, where the grid lines represent lines with constant α and θ in the final parameterization. Initially, H is maped onto K in Figure 5.6(b) with the texture mapped from H. Due to our geometric initialization of θ, the mapping appears to be a global parameterization. However, in regions of H where surface geometry changes more abruptly, such as areas near the tips, θ is not well-behaved and shows serious distortion (see the right side of Figure 5.6(b)). This also causes some overlapping of the initial parameterization from H onto K. Therefore some optimization is required.

After optimizing the initial parameterization using Algorithm 4, the final parameterization result is shown in Figure 5.6(c). The distortion near the tips disappears and the overlapping regions are fixed by the algorithm. The final parameterization is global, smooth and diffeomorphic. This shows that our initial parameterization is very close to optimal. From the plot of the energy functional against the number of iterations in Figure 5.7, our algorithm has clearly converged.

5.3. Distortion Control in Eigen-Harmonic Parameterizations. In this subsection, we show that distortion is well-controlled in eigen-harmonic parameteri-

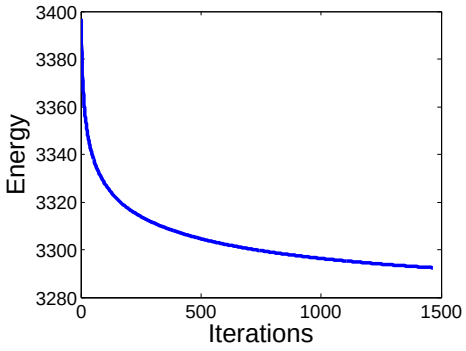

FIG. 5.7. *A plot of the energy functional against the number of iterations in computing the final parameterization in Figure 5.6(c).*

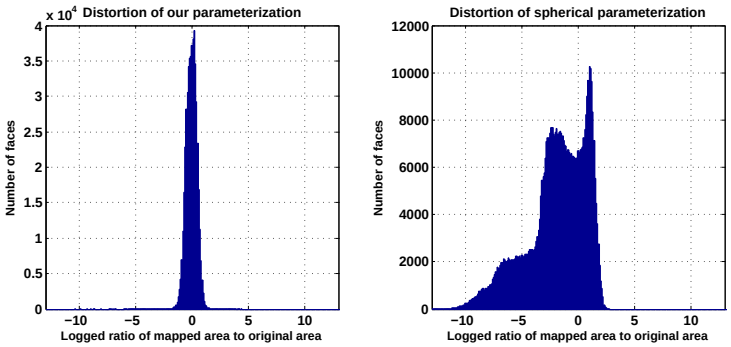

FIG. 5.8. *Distortion comparison between EHP and mapping the same HC surface onto a sphere using conformal mapping.*

zations (EHP). To illustrate this point, we compare the areal expansion factors using our method and mapping HC surfaces conformally onto spheres. We randomly pick 20 HC surfaces of AD patients and 20 HC surfaces of normal subjects for this test. In our method, we map these HC surfaces onto their parameter domains using EHP, while in the other method, we map these HC surfaces conformally onto spheres of the same surface areas. We compute the ratio of the mapped area to the original area for each triangle in the original meshes and plot its distribution under the two methods in Figure 5.8. Since all HC surfaces are triangulated evenly, a histogram of the area expansion ratio gives us a good idea of the area distortion caused by different methods. A good parameterization should preserve the area of the mapping well and the area expansion factors should be close to 1, as far as possible.

In Figure 5.8, histograms showing the number of triangles against the logorithm of the area expansion factors are plotted. In the left histogram for EHP, the triangles lie highly concentrated around 0, which means they are being mapped onto triangles of similar areas (since it means the area expansion ratio is $e^0 = 1$). In contrast, from the histogram for conformal mapping on the right, the distribution shows a huge dispersion and is skewed towards the left. Some triangles are shrinking to as little as e^{-10} times their original area. This shows that EHP controls area distortion better than conformal parametrization.

Besides area distortion, we also compare the consistency of the mapped intrinsic

FIG. 5.9. *Comparison of eigen-harmonic parameterization with conformal parameterization onto sphere.*

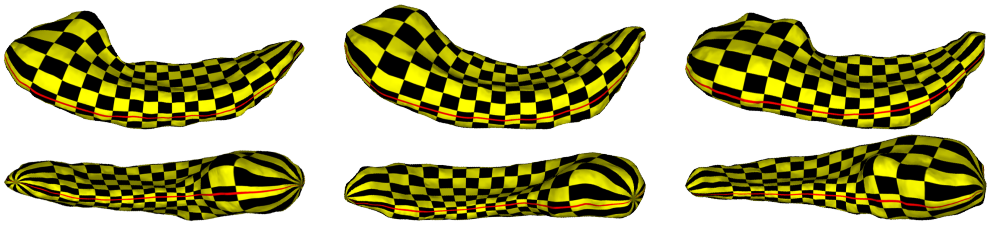

FIG. 5.10. *The front and back of three HC surfaces textured with checkerboard pattern according to their parameterizations in EHP.*

feature curves using these two methods. In Figure 5.9, we plot the results of these two parameterizations. As we can see, a HC surface is smoothly mapped onto our parameter domain, with IFC1 and IFC2 mapped onto $\{\theta = 0\}$ and $\{\theta = \pi\}$ respectively. If we map it conformally onto a sphere of equal area, both IFC1 and IFC2 are not mapped onto consistent locations, making registration difficult. We may enforce such correspondence by mapping IFC1 and IFC2 onto latitudes $\{\theta = 0\}$ and $\{\theta = \pi\}$ of the sphere, but we can no longer expect the mapping to be conformal. To make the mapping as conformal as possible, harmonic map has to be computed. However, since harmonic map is also used in EHP to map HC surfaces onto parameter domains matching the geometry of HC surfaces, our algorithm will always induce less distortion than mapping onto sphere while keeping feature curves fixed.

5.4. HC Shape Analysis using Eigen-Harmonic Registrations. In this subsection, we demonstrate how our algorithms can be used to register HC surfaces consistently for HC shape morphometry. Using EHP, we parameterize HC surfaces onto $[0, 1] \times [0, 2\pi)$. This automatically registers all HC surfaces using their intrinsic surface geometry. In Figure 5.10, the front and back of three HC surfaces are shown from left to right. They are all textured with the same checkerboard pattern according to their parameterizations in EHP. The grid lines of the checkerboard pattern correspond to lines with constant α and θ, and both IFC1 and IFC2 are colored in red. As we can see, although every HC surface displays a distinctive geometry, our algorithms can still smoothly parameterize them and register IFC1 and IFC2 consistently. Distortion is also well controlled, as no texture is largely sketched. This gives us a good correspondence for HC shape morphometry.

Using EHP, each point on a HC surface is mapped to a point on an elliptic cross section of its tubular domain with the same circumference as the eigenloop it's on.

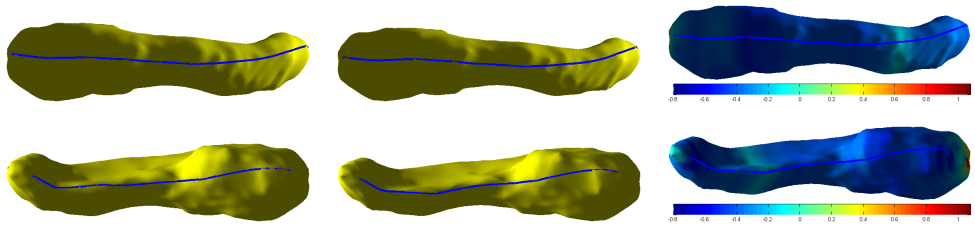

FIG. 5.11. *The result of detecting HC atrophy using EHP. The figures on the left show the original HC surface. The figures in the middle show the artificially shrinked HC surface from the original HC surface along the normal direction. The figures on the right show the change in distance from the corresponding points on the tubular domains to their axises. Most of the areas except areas near the tips show a decrease in the distance, indicating that the shrinkage is successfully detected by EHP.*

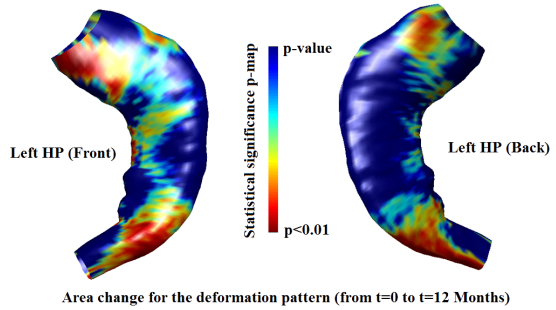

FIG. 5.12. *Results of p-test for HC surfaces of 47 normal and 22 AD subjects.*

Using the change of the distance from the mapped point to the axis of the tubular domain, we can effectively study HC surface atrophy well known to occur in patients with Alzheimer's disease. To demonstrate this property, we choose an HC surface and shrink it along the normal direction. Then we compute the EHP of both surfaces, and measure the change of the distance from the corresponding points on the tubular domains to their axises. As we can see from the result shown in Figure 5.11. EHP successfully captures a decrease of distance from corresponding points on the tubular domains to their axises. This shows that HC atrophy can be effectively detected by EHP.

To study which areas of the HC surface show the most statistically significant group differences in the shape changes over time (between subjects with AD and normal subjects), we perform a t-test of area change ratio between two different times in a random group of 47 normal subjects and 22 AD subjects. The resulting p-values are plotted in Figure 5.12. Areas near the head and the tip show more statistically significant change in area ratio. Tests can be run using other geometric quantities or even clinical data such as cognitive scores, age, sex, prognosis, or measures of pathology in cerebrospinal fluid [17]. Our consistent registration using intrinsic geometry could improve the ability of medical researchers to perform HC surface analysis in large populations.

6. Conclusion. In this paper, we proposed an algorithm to find two intrinsic feature curves according to the intrinsic geometry of HC surfaces, and labeled them as IFC1 and IFC2. We constructed an initial parameterization of HC surfaces using the first non-trivial LB eigenfunction as the longitudinal coordinate α, and estimated

the azimuthal coordinate θ from IFC1 and IFC2. Based on surface geometry, we constructed a parameter domain for each HC surface. We further smoothed the parameterization by minimizing the harmonic energy of the mapping from the HC surface onto its parameter domain, while keeping IFC1 and IFC2 mapped onto $\{\theta = 0\}$ and $\{\theta = \pi\}$ respectively. This completes the construction of the eigen-harmonic parameterization (EHP).

We showed that all our algorithms converged successfully and produced intrinsic feature curves and smooth parameterizations as desired. We demonstrated how IFC1 and IFC2 can be used to detect atrophy on HC surfaces, and how they can be used to extract conformal modules from the front and back of HC surfaces, which are intrinsic surface properties. We compared the distortion of our parameterization with the method of mapping HC surfaces conformally on spheres, and found that our method preserves area well, while the other method causes severe shrinking of some mapped areas. We also showed that the other method could not map IFC1 and IFC2 to consistent locations while keeping the mapping conformal. We illustrated how we can give consistent parameterization for HC surfaces with distinctive surface geometry. Using EHP, we demonstrated how HC shape morphometry can be carried out by performing a pointwise t-test on the area change ratio between two different times in 47 normal subjects, compared to 22 AD subjects.

In medical imaging, many structures of interest have elongated tubular shapes, including the deep nuclei of the brain, blood vessels, and parts of the skeleton. Therefore, we believe our registration may also be effectively applied to other such structures, where a geometrically intrinsic registration is helpful. In the future, we will explore such possibility by applying our algorithms to different kinds of subjects and applications where shape morphometry is needed.

Appendix. In this part, we compute the descent directions used in Algorithm 1 and Algorithm 4. First of all, we compute the coefficients α_i's and β_i's that give the steepest descent to $E(V_{tmp}, W_{tmp})$ in Algorithm 1. Recall that $V_{tmp} = \{v_0 + t\alpha_0 d_0, \ldots, v_n + t\alpha_n d_n\}$, $W_{tmp} = \{w_0 + t\beta_0 e_0, \ldots, w_n + t\beta_n d_n\}$, where d_i's and e_i's are unit tangential vectors along the eigen-loops containing v_i's and w_i's respectively. Also, E is defined as

$$E(V, W) = \frac{1}{n+1} \sum_{i=0}^{n} |v_i - w_i| - c_1 \sum_{i=0}^{n-1} |v_{i+1} - v_i| - c_2 \sum_{i=0}^{n-1} |w_{i+1} - w_i|. \tag{6.1}$$

Before computing the descent directions, we state the following identity without proof:

$$\frac{d|v + tw|}{dt}|_{t=0} = \frac{v \cdot w}{|v|^2}, \tag{6.2}$$

where v and w are vectors and t is a real variable. Now we evaluate

$$\begin{aligned} \frac{d}{dt} E(V_{tmp}, W_{tmp})|_{t=0} = &\sum_{i=0}^{n} \nabla_{v_i} E(V_{tmp}, W_{tmp})|_{t=0} \cdot (\alpha_i d_i) \\ &+ \sum_{i=0}^{n} \nabla_{w_i} E(V_{tmp}, W_{tmp})|_{t=0} \cdot (\beta_i e_i). \end{aligned} \tag{6.3}$$

To minimize E with a positive step t, the descent direction of α_i has to be given by

$$\begin{aligned}\alpha_i &= -\nabla_{v_i} E(V_{tmp}, W_{tmp})|_{t=0} \cdot d_i \\ &= -\frac{d}{dt} E(v_0, \ldots, v_i + td_i, \ldots, v_n, w_0, \ldots, w_n)|_{t=0} \\ &= -(\frac{1}{n+1}\frac{d}{dt}|v_i + td_i - w_i| - c_1\frac{d}{dt}|v_i + td_i - v_{i-1}| - c_2\frac{d}{dt}|v_{i+1} - v_i - td_i|)|_{t=0} \\ &= -\frac{1}{n+1}\frac{(v_i - w_i)\cdot d_i}{|v_i - w_i|^2} + c_1\frac{(v_i - v_{i-1})\cdot d_i}{|v_i - v_{i-1}|^2} - c_1\frac{(v_{i+1} - v_i)\cdot d_i}{|v_{i+1} - v_i|^2},\end{aligned} \tag{6.4}$$

where the second term does not appear for $i = 0$ and the third term does not appear for $i = n$. Similarly β_i is given by

$$\beta_i = -\frac{1}{n+1}\frac{(w_i - v_i)\cdot e_i}{|w_i - v_i|^2} + c_2\frac{(w_i - w_{i-1})\cdot e_i}{|w_i - w_{i-1}|^2} - c_2\frac{(w_{i+1} - w_i)\cdot e_i}{|w_{i+1} - w_i|^2}, \tag{6.5}$$

where the second term does not appear for $i = 0$ and the third term does not appear for $i = n$.

For Algorithm 4, we compute the coefficients δ_i's that give the steepest descent to $E(\phi_1 + t\delta_1, \ldots, \phi_m + t\delta_m)$. Recall that

$$\begin{aligned}E(\phi_1, \ldots, \phi_m) &= \sum_{i=1}^{3} E_{\text{harmonic}}(\Phi_i) \\ &= \sum_{i=1}^{3}\frac{1}{2}\sum_{(v_j, v_k)\in\mathcal{E}} L_{v_j, v_k}(\Phi_i(v_j) - \Phi_i(v_k))^2.\end{aligned} \tag{6.6}$$

We evaluate

$$\frac{d}{dt}E(\phi_1 + t\delta_1, \ldots, \phi_m + t\delta_m)|_{t=0} = \sum_{i=1}^{m}\frac{\partial}{\partial\phi_i}E(\phi_1, \ldots, \phi_m)\delta_i. \tag{6.7}$$

To minimize E with a positive step t, the descent direction of δ_i has to be given by

$$\begin{aligned}\delta_i &= -\frac{\partial}{\partial\phi_i}E(\phi_1, \ldots, \phi_m) \\ &= -\frac{\partial}{\partial\phi_i}\sum_{j=1}^{3}\frac{1}{2}\sum_{(v_k, v_l)\in\mathcal{E}} L_{v_k, v_l}(\Phi_j(v_k) - \Phi_j(v_l))^2 \\ &= -\frac{\partial}{\partial\phi_i}\sum_{j=1}^{3}\frac{1}{2}\sum_{v_k\in\text{Nbr}(v_i)} L_{v_i, v_k}(\Phi_j(v_i) - \Phi_j(v_k))^2 \\ &= -\sum_{j=1}^{3}\sum_{v_k\in\text{Nbr}(v_i)} L_{v_i, v_k}(\Phi_j(v_i) - \Phi_j(v_k))\frac{\partial}{\partial\phi_i}\Phi_j(v_i).\end{aligned} \tag{6.8}$$

Note that $\Phi(v_i) = (a(v_i)\cos(\phi(v_i)), b(v_i)\sin(\phi(v_i)), h\alpha(v_i))$. Therefore

$$\begin{aligned}\delta_i = \sum_{v_k\in\text{Nbr}(v_i)} L_{v_i, v_k}[&(\Phi_1(v_i) - \Phi_1(v_k))a(v_i)\sin(\phi(v_i)) \\ &- (\Phi_2(v_i) - \Phi_2(v_k))b(v_i)\cos(\phi(v_i))].\end{aligned} \tag{6.9}$$

REFERENCES

[1] M. Berger, P. Gauduchon, and E. Mazet, *Le spectre d'une variété Riemannienne*, Lecture notes in mathematics, vol. 194. Springer-Verlag, Berlin, 1971.

[2] A. Burggren, M. Zeineh, A. Ekstrom, M. Braskie, P. Thompson, G. Small, and S. Bookheimer, *Reduced cortical thickness in hippocampal subregions among cognitively normal apolipoprotein E e4 carriers*, NeuroImage, 41 (2008), pp. 1177 – 1183.

[3] I. Chavel, *Eigenvalues in Riemannian geometry*, Pure and applied mathematics. Academic Press, Orlando, 1971.

[4] S. Durrleman, X. Pennec, A. T. P. Thompson, and N. Ayache, *Inferring brain variability from diffeomorphic deformations of currents: An integrative approach*, Medical Image Analysis, 12 (2008), pp. 626 – 637. Special issue on the 10th international conference on medical imaging and computer assisted intervention - MICCAI 2007.

[5] G. H. Golub and Q. Ye, *An inverse free preconditioned krylov subspace method for symmetric generalized eigenvalue problems*, SIAM J. Sci. Comput., 24 (2002), pp. 312–334.

[6] X. Gu, Y. Wang, T. Chan, P. Thompson, and S.-T. Yau, *Genus zero surface conformal mapping and its application to brain surface mapping*, Medical Imaging, IEEE Transactions on, 23 (2004), pp. 949 –958.

[7] A. Iserles, *A First Course in the Numerical Analysis of Differential Equations, 2nd Edition*, Cambridge University Press, 1998.

[8] A. A. Joshi, D. W. Shattuck, P. M. Thompson, and R. M. Leahy, *Cortical surface parameterization by p-harmonic energy minimization*, in in IEEE ISBI, 2004, pp. 428–431.

[9] A. Leow, C. Yu, S. Lee, S. Huang, H. Protas, R. Nicolson, K. Hayashi, A. Toga, and P. Thompson, *Brain structural mapping using a novel hybrid implicit/explicit framework based on the level-set method*, NeuroImage, 24 (2005), pp. 910 – 927.

[10] N. Leporé, Y. Shi, F. Lepore, M. Fortin, P. Voss, Y.-Y. Chou, C. Lord, M. Lassonde, I. D. Dinov, A. W. Toga, and P. M. Thompson, *Pattern of hippocampal shape and volume differences in blind subjects*, NeuroImage, 46 (2009), pp. 949–957.

[11] J. Lin, N. Salamon, A. Lee, R. Dutton, J. Geaga, K. Hayashi, A. Toga, J. Engel, and P. Thompson, *3D pre-operative maps of hippocampal atrophy predict surgical outcomes in temporal lobe epilepsy*, Neurology, 65 (2005), pp. 1094–1097.

[12] N. Lord, J. Ho, B. Vemuri, and S. Eisenschenk, *Simultaneous registration and parcellation of bilateral hippocampal surface pairs for local asymmetry quantification*, Medical Imaging, IEEE Transactions on, 26 (2007), pp. 471 –478.

[13] L. M. Lui, S. Thiruvenkadam, Y. Wang, T. Chan, and P. Thompson, *Optimized conformal parameterization of cortical surfaces using shape based matching of landmark curves*, in SIAM Journal of Imaging Sciences, vol. 3, 2010, pp. 52–78.

[14] L. M. Lui, Y. Wang, T. Chan, and P. M. Thompson, *Brain anatomical feature detection by solving partial differential equations on general manifolds*, in Discrete and Continuous Dynamical Systems B, vol. 7, 2007, pp. 605–618.

[15] ———, *Landmark constrained genus zero surface conformal mapping and its application to brain mapping research*, in Applied Numerical Mathematics, vol. 57, 2007, pp. 847–858.

[16] L. M. Lui, T. W. Wong, X. Gu, P. Thompson, T. Chan, and S.-T. Yau, *Hippocampal shape registration using beltrami holomorphic flow*, in Medical Image Computing and Computer Assisted Intervention(MICCAI), vol. 6362, 2010, pp. 323–330.

[17] J. Morra, Z. Tu, L. Apostolova, A. Green, C. Avedissian, S. Madsen, N. Parikshak, A. Toga, C. Jackjr, and N. Schuff, *Automated Mapping of Hippocampal Atrophy in 1-Year Repeat MRI Data from 490 Subjects with Alzheimer's Disease, Mild Cognitive Impairment, and Elderly Controls*, NeuroImage, (2008).

[18] J. H. Morra, Z. Tu, L. G. Apostolova, A. E. Green, C. Avedissian, S. K. Madsen, N. Parikshak, X. Hua, A. W. Toga, C. R. Jack, N. Schuff, M. W. Weiner, and P. M. Thompson, *Automated 3D mapping of hippocampal atrophy and its clinical correlates in 400 subjects with Alzheimer's disease, mild cognitive impairment, and elderly controls.*, Hum Brain Mapp, 30 (2009), pp. 2766–88.

[19] J. H. Morra, Z. Tu, L. G. Apostolova, A. E. Green, C. Avedissian, S. K. Madsen, N. Parikshak, X. Hua, A. W. Toga, C. R. Jack, M. W. Weiner, P. M. Thompson, and Alzheimer's Disease Neuroimaging Initiative, *Validation of a fully automated 3D hippocampal segmentation method using subjects with Alzheimer's disease mild cognitive impairment, and elderly controls.*, NeuroImage, 43 (2008), pp. 59–68.

[20] J. H. Morra, Z. Tu, L. G. Apostolova, A. E. Green, A. W. Toga, and P. M. Thompson, *Comparison of AdaBoost and support vector machines for detecting alzheimer's disease through automated hippocampal segmentation*, IEEE Trans. Med. Imaging, 29 (2010),

pp. 30–43.

[21] T. P.M., *Detection, visualization and animation of abnormal anatomic structure with a deformable probabilistic brain atlas based on random vector field transformations*, Medical Image Analysis, 1 (September 1997), pp. 271–294(24).

[22] M. Reuter, F. Wolter, M. Shenton, and M. Niethammer, *Laplace-Beltrami eigenvalues and topological features of eigenfunctions for statistical shape analysis.*, Computer aided design, 41 (2009), pp. 739–755.

[23] M. Reuter, F.-E. Wolter, and N. Peinecke, *Laplace-Beltrami spectra as 'Shape-DNA' of surfaces and solids*, Computer-Aided Design, 38 (2006), pp. 342–366.

[24] Y. Shi, R. Lai, K. Kern, N. Sicotte, I. Dinov, and A. W. Toga, *Harmonic surface mapping with Laplace-Beltrami eigenmaps*, in Proceedings of the 11th International Conference on Medical Image Computing and Computer-Assisted Intervention, Part II, MICCAI '08, Berlin, Heidelberg, 2008, Springer-Verlag, pp. 147–154.

[25] Y. Shi, P. M. Thompson, I. Dinov, S. Osher, and A. W. Toga, *Direct cortical mapping via solving partial differential equations on implicit surfaces*, Medical Image Analysis, 11 (2007), pp. 207 – 223.

[26] P. Thompson and A. W. Toga, *A surface-based technique for warping three-dimensional images of the brain.*, IEEE transactions on medical imaging, 15 (1996), pp. 402–417.

[27] P. M. Thompson, K. M. Hayashi, G. I. de Zubicaray, A. L. Janke, S. E. Rose, J. Semple, M. S. Hong, D. H. Herman, D. Gravano, D. M. Doddrell, and A. W. Toga, *Mapping hippocampal and ventricular change in Alzheimer disease*, NeuroImage, 22 (2004), pp. 1754 – 1766.

[28] P. M. Thompson, A. W. Toga, C. Johnson, and D. P. Thompson, *A framework for computational anatomy*, Computing and Visualization in Science, 5 (2002), pp. 13 – 34.

[29] Y. Wang, M.-C. Chiang, and P. M. Thompson, *Automated surface matching using mutual information applied to Riemann surface structures*, in Medical Image Computing and Computer-Assisted Intervention MICCAI 2005, J. Duncan and G. Gerig, eds., vol. 3750 of Lecture Notes in Computer Science, Springer Berlin / Heidelberg, 2005, pp. 666–674.

[30] W. Yalin, L. M. Lui, X. Gu, K. Hayashi, T. Chan, P. Thompson, and S.-T. Yau, *Brain surface conformal parameterization using riemann surface structure*, IEEE Transaction of Medical Imaging, 26 (2007), pp. 853–865.

[31] S. Yoshizawa, A. Belyaev, and H.-P. Seidel, *Fast and robust detection of crest lines on meshes*, in Proceedings of the 2005 ACM symposium on Solid and physical modeling, SPM '05, New York, NY, USA, 2005, ACM, pp. 227–232.

[32] M. M. Zeineh, S. A. Engel, P. M. Thompson, and S. Y. Bookheimer, *Unfolding the human hippocampus with high resolution structural and functional MRI.*, Anat Rec, 265 (2001), pp. 111–20.

[33] M. M. Zeineh, S. A. Engel, P. M. Thompson, and S. Y. Bookheimer, *Dynamics of the hippocampus during encoding and retrieval of face-name pairs*, Science, 299 (2003), pp. 577–580.

[34] W. Zeng, L. M. Lui, X. Gu, and S.-T. Yau, *Shape analysis by conformal modules*, Methods and Applications of Analysis, 15 (2008), pp. 539–556.